Proceedings, 11th International Conference on Clouds & Precipitation, Montreal, CANADA, **2**, Aug. 17-21, 1992. 750-753.

THE HEAT BUDGET OF A MIDLATITUDE SQUALL LINE DETERMINED FROM A THERMODYNAMIC AND MICROPHYSICAL RETRIEVAL

Scott A. Braun and Robert A. Houze, Jr.

Department of Atmospheric Sciences, AK-40
University of Washington
Seattle, WA 98195 USA

1. INTRODUCTION

The cumulus-environment interaction is frequently described through budgets for heat and moisture, generally with data collected at scales comparable to, or somewhat larger than, the convective systems. In a recent study, Gallus and Johnson (1991, GJ hereafter) examined the heat budget of the 10-11 June 1985 PRE-STORM[1] squall line using composites of rawinsonde data from the National Weather Service and supplemental sites. The composite data was interpolated to grids with spacing of 0.5° latitude and longitude. This resolution makes it difficult to delineate the convective and mesoscale contributions to the heat budget since convective region velocities can be aliased into the trailing stratiform precipitation region. In addition, this evaluation of the heat budget takes advantage of only a small portion of the data (mainly rawinsondes) from the PRE-STORM network, which was designed to document processes on a wide range of scales simultaneously (Cunning 1986). The ultimate goal of our research is to combine as many of these data sources as possible to obtain a more complete analysis of all the processes contributing to the heat budget than can be obtained from the soundings alone. In particular, we wish to resolve the processes occurring on various scales within the storm. As part of this effort, we present some results of calculations that derive heat budget results for the 10-11 June squall line from dual-Doppler-radar data, which have the resolution to distinguish the separate processes occurring in the convective, transitional, and stratiform regions of the storm. Wind fields have been synthesized previously from the dual-Doppler measurements (Biggerstaff and Houze 1991). Here we apply a retrieval technique to the synthesized wind field to obtain the corresponding temperature and microphysical fields. A heat budget is then formed by combining the synthesized wind field and retrieved thermodynamic and microphysical fields. These calculations indicate the utility of the retrieval technique as a tool for deducing the heating that is associated with convective and mesoscale processes. Although this analysis has the disadvantage that only a small portion of the entire mesoscale convective system can be studied, it has the advantage of resolving the heating down to the scale of the convective motions so that contributions from different regions of the storm (convective, transitional, stratiform) can be deduced. Eventually, results obtained by the retrieval method can be combined with those obtained by other techniques, such as sounding analysis, to obtain a comprehensive study of the heat budget of the storm.

2. RETRIEVAL METHODOLOGY

The retrieval method used for the present analysis closely follows that of Hauser et al. (1988) and Marecal and Hauser (1991). The microphysical fields are obtained by using the bulk microphysical parameterizations of Lin et al. (1983) and Rutledge and Hobbs (1983), and solving two-dimensional, steady-state conservation equations for the microphysical variables.

[1] PRE-STORM is an acronym for Oklahoma-Kansas Preliminary Regional Experiment for the Stormscale Operational and Research Meteorology Program-Central Phase.

Temperature and pressure are determined in a manner similar to the dynamic method of Hauser et al. (1988). For the present case, the Coriolis terms are included in the momentum equations. Since we perform the retrieval for both the convective and stratiform precipitation regions, the temperature and pressure are deduced using the variational approach of Roux and Sun (1990) which was shown by Sun and Houze (1992) to reproduce adequately the temperature field in the stratiform precipitation region.

3. DATA

The three-dimensional wind field used in the retrieval is taken from a composite of dual-Doppler-derived wind fields for the northern portion of the 10-11 June 1985 PRE-STORM squall line during the mature stage of the system. The composite data set has horizontal and vertical resolution of 3 and 0.5 km, respectively (see Biggerstaff and Houze (1992) for details).

An average vertical cross section oriented normal to the squall line was obtained by averaging over a 60-km wide strip perpendicular to the line. Figure 1a shows the mean reflectivity and vectors of the two-dimensional wind in the plane of the cross section, and Figure 1b shows the average vertical velocity. The cross section is characterized by a 60-km wide leading convective line, followed by a region of stratiform precipitation nearly 150 km wide. The transition zone, defined by the low-level reflectivity minimum between $x \approx 35$ and 60 km, separates the convective and stratiform

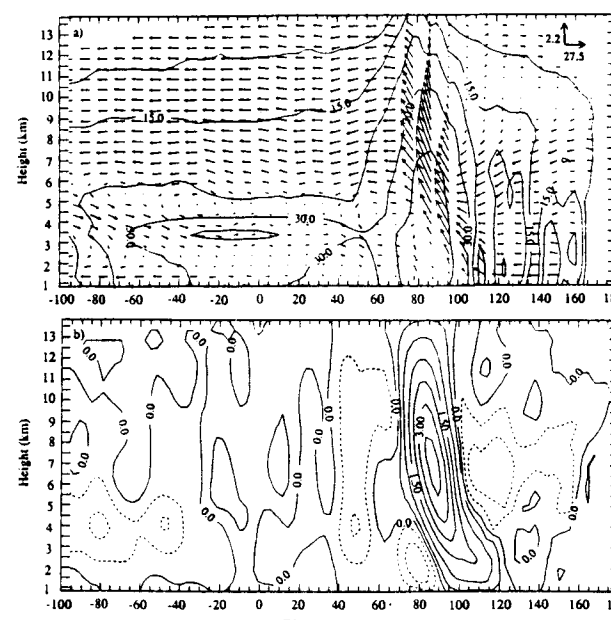

Fig. 1 (a) Along-line averaged radar reflectivity (contoured every 7.5 dBZ) and wind vectors in the plane of the cross section. The arrows in the upper right corner represent the arrow scales corresponding to 2.2 m s^{-1} for the vertical velocity and 27.5 m s^{-1} for the horizontal velocity. (b) Vertical velocity (m s^{-1}) with contours drawn at -0.5, -0.25, 0., 0.25, 0.75, 1.5, 2.25, 3.0, and 3.75 m s^{-1}.

precipitation regions. The velocity field shows strong front-to-rear (FTR) flow in the convective region and above about 5.5 km in the trailing stratiform region. A layer of rear-to-front (RTF) velocity is seen near the melting level in the stratiform rain region. It descends to near the surface in the convective region. Weak RTF flow also occurred at upper-levels ahead of the convective tower, while FTR flow occurred at low levels under the trailing stratiform precipitation. The vertical velocity field is characterized by strong ascent in the leading convective line, but relatively weak ascent in the stratiform region. Substantial descent is present: 1) at midlevels ahead of the convective line, 2) at low levels in the convective region, 3) through the depth of the troposphere in the transition zone, and 4) near the melting level in the stratiform region, particularly in the region behind the secondary band.

The mesoscale ascent above the melting level in the stratiform region is very weak. Comparison of the vertical velocity field to the EVAD vertical velocity analysis of Rutledge et al. (1988) suggests that either the procedure used to obtain the composite field substantially reduced the strength of the mesoscale updraft, or the 60-km wide strip did not sample the mesoscale updraft adequately. In either case, the mesoscale updraft heating will not be well represented in the present results. This is a limitation of the current data set and will require further examination at another time.

4. RESULTS

The retrieved potential temperature perturbation is shown in Figure 2. At low levels, a cold pool extending up to approximately 3.5 km exists as a result of the melting of graupel and evaporation of rain. The lowest temperature perturbations (< –5°K) are located in the vicinity of the convective downdraft. Although the retrieval diagnoses cold air at low levels in the stratiform precipitation region generally well, it is unable to reproduce all of the details of the low-level temperature structure. Comparison of a retrieved stratiform region temperature profile with low-level profiles from rawinsonde data suggests that the cold pool in this region should be somewhat deeper and that lapse rates below the melting level should be steeper. The retrieved melting level is somewhat higher (4.3 km) than the observed level of 3.9 km. However, this difference is less than the vertical grid spacing.

Warm air extends from about 3.5 km up to nearly 10.8 km in the convective region and to about 9 km ahead of and behind the convective region. The cold perturbations above 9-10 km may reflect the transport of low-level air above its equilibrium level. There is a minimum in temperature near x=10 km at storm top, located approximately 70 km behind the top of the convective line. This is in good agreement with the observation of Zipser (1988) that the satellite infrared temperature minimum was located 50-100 km behind the leading convective line during the mature phase of the squall line.

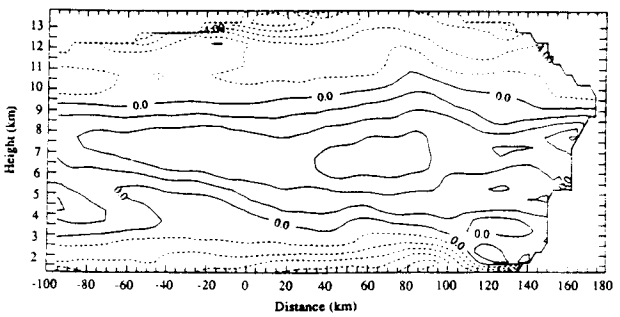

Fig. 2 Retrieved potential temperature perturbation with respect to the pre-squall environment. Contour interval is 1°K. Solid (dashed) contours indicate positive (negative) values.

The heating rate Q_1 is defined following GJ as

$$Q_1 = \bar{u}\frac{\partial \bar{s}}{\partial x} + \bar{w}\frac{\partial \bar{s}}{\partial z}$$
$$= Q_r + L_v(\bar{c} - \bar{e}) + (L_v + L_f)(\bar{d} - \bar{s}^*)$$
$$+ L_f(\bar{f} - \bar{m}) - \frac{\partial}{\partial x}\overline{u's'} - \frac{1}{\bar{\rho}}\frac{\partial}{\partial z}\bar{\rho}\overline{w's'} \qquad (1)$$

where $s = c_pT + gz$ is the dry static energy, c_p is the specific heat at constant pressure, L_v and L_f are the latent heats of vaporization and fusion, Q_r is the radiative heating rate, and c, e, d, s^*, f, and m are the rates of condensation, evaporation, deposition, sublimation, freezing, and melting, respectively. The overbars represent averages over 3 km x 3 km x 0.5 km volumes centered on the grid points while the primes denote the deviations from these averages. The last two terms in (2) then represent the horizontal and vertical convergences of the eddy heat flux by unresolved processes.

In this study, Q_1 is determined from the left side of (2) and c,e,d, and s^* are determined from

$$\vec{V} \bullet \nabla \bar{q}_v = -\delta(\bar{c} - \bar{e}) - (1-\delta)(\bar{d} - \bar{s}^*) \qquad (2)$$

where δ is 1 for $T > 0$°C and zero otherwise, and f and m are determined from the appropriate bulk parameterization terms. No attempt is made to deduce the remaining terms on the right side of (2) explicitly. In the profiles shown below, these terms will be lumped together and determined as a residual (Q_1 – latent heating). Note that this residual may also reflect the amount of error in the retrieval.

The Q_1 field, as determined by the advection of dry static energy, is shown as a two-dimensional line-normal cross section in Fig. 3. Strong heating occurs in the convective updraft with a maximum of 60°K h^{-1} at 6.4 km (464 mb), but relatively little heating occurs in the mesoscale updraft. At midlevels ahead of the convective updraft and at low levels in the convective downdraft, cooling rates greater than 10°K h^{-1} occur. In the transition and stratiform regions, peak cooling rates associated with evaporation, sublimation, and melting occur between roughly 3 and 5 km.

The contributions to the total heating rate, Q_1, of the convective, transition, and stratiform regions can be determined using a decomposition technique similar to that used by Houze (1982). We let

$$Q_1 = \sigma_c Q_{1c} + \sigma_t Q_{1t} + \sigma_m Q_{1m} + \sigma_f Q_{1f} \qquad (3)$$

where $Q_{1c}(\sigma_c)$, $Q_{1t}(\sigma_t)$, $Q_{1m}(\sigma_m)$, and $Q_{1f}(\sigma_f)$ are the heating rates (fractional areas) of the convective region, transition zone, stratiform region, and forward anvil region (x > 135 km), respectively. Since the heating in the region x > 135 km makes only a minor contribution to the total

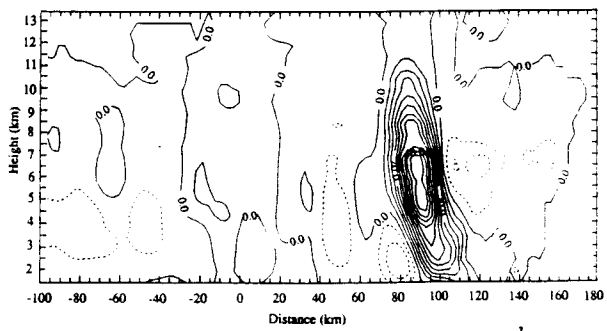

Fig. 3 Apparent heat source, Q_1, contoured every 5 °K h^{-1}.

heating (see Fig. 3), a profile for Q_{1f} will not be shown. Profiles for the first three regions are shown in Fig. 4.

In the convective region, except near cloud top, there is net heating throughout the troposphere, with peak heating near 5 km. This differs from the GJ convective profiles in two ways: 1) the profiles of GJ show net cooling at low levels, whereas the results from the retrieval show that heating by condensation at low levels in the convective updraft is stronger than the cooling produced in the convective downdraft; and 2) the peak in the average heating rate determined here occurs 1.5-3.5 km lower than the double-peaked profile of GJ (for 0300 UTC). The lower peak in the heating rate is due partially to the cooling at midlevels just ahead of the convective updraft which was included in the convective region average. Such cooling was apparently not included in the average profile in GJ.

The transition-zone profile is characterized by cooling throughout the troposphere with one cooling maximum located at 3.9 km and a second, weaker maximum near 8.4 km. This is consistent with the double-peaked structure of the transition-zone subsidence found by Biggerstaff and Houze (1992).

Since the mesoscale updraft is poorly represented in the composite analysis, the stratiform region profile differs markedly from that of GJ. In their study, the stratiform region at 0300 UTC is characterized by a strong heating maximum near 450 mb (near 6.4 km) and relatively weak cooling below 700 mb (3 km). Our results show relatively little heating within the mesoscale updraft. On the other hand, substantial cooling occurs through a deep layer from the surface to 6 km with peak cooling at 3.4 km. In GJ, the cooling above 3 km is more than balanced by heating in their main updraft.

In the total heating profile, Q_1, there is heating throughout the troposphere except for shallow layers between 2.5-3.5 km and above 12 km. Below 4 km, the significant cooling by melting and evaporation in the stratiform region and transition zone nearly cancels the heating by condensation in the convective updraft. At mid-to-upper levels, the total heating profile is probably not representative of the actual total heating since the mesoscale updraft is either not sampled adequately or is smoothed out by the analysis procedure (see above).

Figure 5 shows the different components of the total heating according to the terms on the right side of (1). The profile labeled *R* represents the difference Q_1–'latent heating' and should reflect the heating rates associated with radiative processes, the convergence of the eddy heat flux, and any residual errors in the temperature and microphysical retrievals or in the assumption of steady-state conditions. The condensation and deposition profile peaks just under 6 km and decreases rapidly to zero above 7 km. There is additional heating of approximately 0.3°K h^{-1} by the freezing of rain and cloud water between 4.3 km and 9 km decreasing to zero at cloud top. Below 5 km the evaporation and sublimation profile is dominated by the cooling in mesoscale and transition zone downdrafts while above this level, the cooling is largely associated with the subsidence just ahead of the convective updraft as well as with the subsidence in the upper part of the transition zone. Thus, cooling occurs, rather substantially, through the depth of the whole troposphere.

Near 4 km, the curve *m* in Fig. 5 indicates that the cooling associated with melting hydrometeors has a magnitude approaching that associated with evaporation. Figure 6 shows the spatial distribution of cooling and heating rates by melting and freezing determined from the microphysical retrieval. The most striking feature is the strong cooling by melting (up to –9°K h^{-1}) that occurs in the convective region. It has been previously recognized that a concentrated melting layer occurs in the stratiform region. These results suggest that a similar, and even more intense, melting layer may occur in the convective region. Actually, the high cooling rates in Fig. 6 extend into the transition zone in the retrieval, but this is an artificial result of an inability of the microphysical retrieval to reproduce well the precipitation minimum in the transition zone. The strong cooling rates are associated with the melting of graupel falling from the upper parts of the convective cells in the squall line. The strong melting layer in the convective-transition region indicates that melting probably played a substantial role in the thermodynamics of this part of the storm by decreasing the potential temperature, and the equivalent potential temperature, of the air parcels descending in the convective downdrafts. This increase in

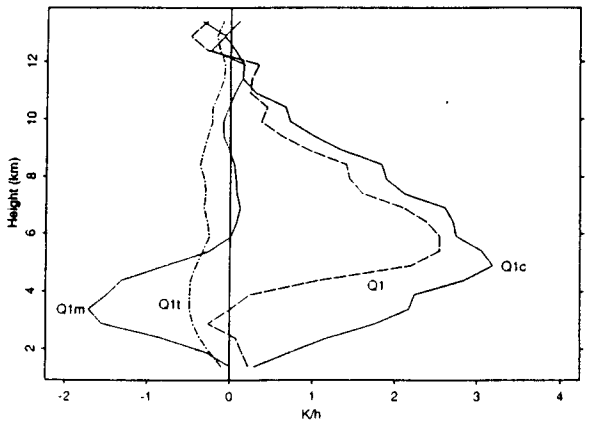

Fig. 4 Vertical distribution of the apparent heat source, Q_1, averaged over the convective region (Q_{1c}), transition zone (Q_{1t}), stratiform region (Q_{1m}), and total domain (Q_1). The profiles have been multiplied by the respective fractional areas to facilitate direct comparison.

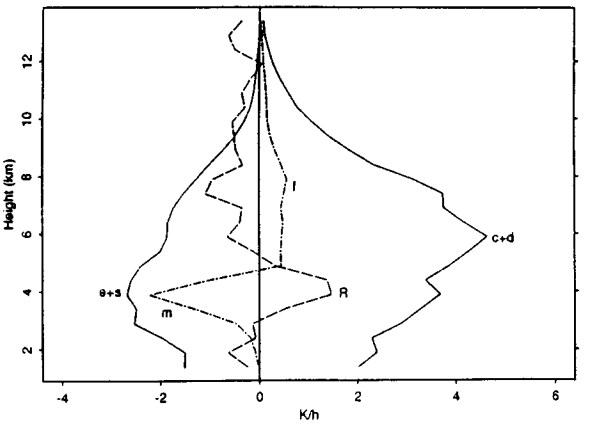

Fig. 5 Vertical distributions of the individual components of the total heating determined from the left side of (2), including condensation and deposition (c+d), evaporation and sublimation (e+s), melting (m), and freezing (f). The profile labeled R is described in the text.

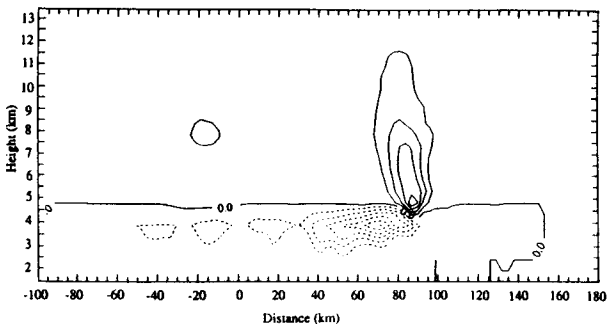

Fig. 6 Heating and cooling rates associated with freezing (solid) and melting (dashed). Contour interval is 1.5°K h^{-1}.

the negative thermal buoyancy can drive stronger downdrafts, as shown by Srivastava (1987). In addition, Szeto et al. (1988) showed that cooling by melting can force significant mesoscale circulations. Melting in the convective-transition region, then, is an additional mechanism for the intensification of the surface cold pool and gust front.

The curve R for Q_1-'latent heating' compares favorably with profiles for radiative cooling and heating by the eddy flux convergence in the "nighttime" simulation of Churchill and Houze (1991). They showed that below the 0°C level, heating due to convective overturning tends to balance partially the cooling by melting and evaporation, while at cloud top, radiative cooling tends to dominate over heating by the eddy flux convergence to produce net cooling.

6. CONCLUSIONS

A thermodynamic and microphysical retrieval was applied to a 60-km wide region of the northern part of the 10-11 June 1985 squall line for the purpose of computing a diagnostic heat budget with data down to the scale of the convective motions. This allowed for a clearer delineation of the convective, transition, and stratiform contributions to the total heating. The retrieval technique enabled us to obtain reasonable estimates of the heating except at mid-to-upper levels in the stratiform region. Of particular interest, we found that the presence of midlevel cooling associated with subsidence immediately ahead of the convective updraft led to a lowering of the peak heating rate in the average convective region heating profile (Q_{1c}). Additional mid-to-upper level cooling occurred within the transition zone. Substantial cooling by melting was found to occur in the rear part of the convective region. This cooling probably acted to reinforce the role of evaporation in the development of the surface cold pool and the gust front.

Acknowledgments: We would like to thank Drs. F. Roux and J. Sun for making the temperature retrieval software available to us, and Dr. M. Biggerstaff for providing us with the synthesized dual-Doppler radar data set used in this study. G. C. Gudmundson edited the manuscript and K. M. Dewar helped draft the figures. This research was sponsored by National Science Foundation grant ATM-610230.

REFERENCES

Biggerstaff, M. I., and R. A. Houze, Jr., 1991: Kinematic and precipitation structure of the 10-11 June 1985 squall line. *Mon. Wea. Rev.*, **119**, 3034-3065.

Biggerstaff, M. I., and R. A. Houze, Jr., 1992: Kinematics and microphysics of the transition zone of a midlatitude squall line system. *J. Atmos. Sci.* (accepted).

Churchill, D. D., and R. A. Houze, Jr., 1991: Effects of radiation and turbulence on the diabatic heating and water budget of the stratiform region of a tropical cloud cluster. *J. Atmos. Sci.*, **48**, 903-922.

Cunning, J. B., 1986: The Oklahoma-Kansas Preliminary Regional Experiment for STORM-central. *Bull. Amer. Meteor. Soc.*, **67**, 1478-1486.

Gallus, W. A., Jr., and R. H. Johnson, 1991: Heat and moisture budget of an intense midlatitude squall line. *J. Atmos. Sci.*, **48**, 122-146.

Hauser, D., F. Roux and P. Amayenc, 1988: Comparison of two methods for the retrieval of thermodynamic and microphysical variables from Doppler-radar measurements: Application to the case of a tropical squall line. *J. Atmos. Sci.*, **45**, 1285-1303.

Houze, R. A., Jr., 1982: Cloud clusters and large-scale vertical motions in the tropics. *J. Meteor. Soc. Japan*, **60**, 396-410.

Lin, Y-L., R. D. Farley and H. D. Orville, 1983: Bulk parameterization of the snow field in a cloud model. *J. Climate Appl. Meteor.*, **22**, 1065-1092.

Marecal, V. and D. Hauser, 1991: Retrieval of thermodynamic and microphysical variables from dual-Doppler-radar measurements in frontal rainbands. *Preprints, 25th Conf. on Radar Meteorology*, 24-28 June 1991, Paris, France, American Meteorological Society, 143-146.

Roux, F. and J. Sun, 1990: Single-Doppler observations of a West African squall line on 27-28 May 1981 during COPT 81: Kinematics, thermodynamics, and water budget. *Mon. Wea. Rev.*, **118**, 1826-1854.

Rutledge, S. A., and P. V. Hobbs, 1983: The mesoscale and microscale structure and organization of clouds and precipitation in midlatitude cyclones, VII: A model for the "seeder-feeder" process in warm frontal rainbands. *J. Atmos. Sci.*, **40**, 1185-1206.

Rutledge, S. A., R. A. Houze, Jr., M. I. Biggerstaff and T. Matejka, 1988: The Oklahoma-Kansas mesoscale convective system of 10-11 June 1985: Precipitation structure and single-Doppler-radar analysis. *Mon. Wea. Rev.*, **116**, 1409-1430.

Srivastava, R. C., 1987: A model of intense downdrafts driven by the melting and evaporation of precipitation. *J. Atmos. Sci.*, **44**, 1752-1773.

Sun, J. and R. A. Houze, Jr., 1992: Validation of a thermodynamic retrieval technique by application to a simulated squall line with trailing stratiform precipitation. *Mon. Wea. Rev.* (April).

Szeto, K. K., R. E. Stewart and C. A. Lin, 1988: Mesoscale circulations forced by melting snow. Part II: Application to meteorological features. *J. Atmos. Sci.*, **45**, 1642 -1650.

Zipser, E. J., 1988: The evolution of mesoscale convective systems: Evidence from radar and satellite observations. *Tropical Rainfall Measurements*, (J. S. Theon and N. Fugono, Eds.), A. Deepak Publishing, Hampton, 159-166.